

## Investigation of electrical and dielectric studies of calcium doped magnesium titanate $[\text{Mg}_{(1-x)}\text{Ca}_x\text{TiO}_3 (x=0, 0.9)]$ ceramics

V. S. Samyuktha<sup>a,\*</sup>, A. G. Sampath Kumar<sup>b</sup>, T. S. Rao<sup>c</sup>, R. P. Suvarna<sup>d</sup>

<sup>a</sup>Department of Physics, Maris Stella College (Autonomous), Vijayawada, India

<sup>b</sup>Department of Physics, Malla Reddy Engineering College(A), Hyderabad-500100, T.S., India

<sup>c</sup>Material Science Lab, Department of Physics, Sri Krishnadevaraya University, Anantapuramu, India

<sup>d</sup>Department of Physics, Jawaharlal Nehru Technological University, Anantapuramu, India

The pure and calcium doped magnesium titanate ceramics were synthesised by conventional solid-state diffusion method. The intension of the present work was to investigate the influence of  $\text{Ca}^{2+}$  on electrical and dielectric properties of the above ceramics. The dielectric constant from room temperature to  $350^\circ\text{C}$  was calculated using HIOKI 3532-50 LCR HiTESTER in the frequency range of 1KHz-1MHz. The dielectric constant at room temperature at a frequency of 1MHz for Calcium doped Magnesium Titanate was found to be and as the concentration of Calcium increases dielectric constant increases. The AC conductivity, Dielectric loss of the samples were measured and thermoelectric properties were studied. XRD studies revealed that the compound exhibits single phase with Orthorhombic structure and space group  $62 : \text{Pbnm}$ .

(Received March 28, 2021; Accepted July 13, 2021)

*Keywords:* Solid state diffusion, Dielectric constant, AC conductivity

### 1. Introduction

Magnesium titanate ceramics play an important role in microwave technologies such as global positioning system operating at microwave frequencies, resonators, filters, antennas for communication system and multilayer capacitors [1-4]. It is a versatile material of low dielectric loss with high quality factor (Q above 20000 at 8GHz) and intermediate dielectric constant ( $\epsilon_r=17$ ) [5]. An  $\text{MgTiO}_3$  ceramic exhibits ilmenite structure with rhombohedral crystal system and belongs to R-3 group [6, 7].  $\text{MgTiO}_3$  are being prepared by various techniques such as thermal decomposition of peroxide precursors, hydrothermal mechano-chemical complexation routes, Sol-gel method, MOSD and auto-igniting combustion technique [8-13], Chemical co-precipitation [14], metalorganic chemical vapour deposition [15]. In this work, the effect of calcium dopant study is studied.

### 2. Experimental procedure

Reagent grade raw materials of  $\text{MgO}$ ,  $\text{TiO}_2$  and  $\text{CaO}$  were used as starting materials. These materials were taken according to the composition and then milled for 12h in a Bill Miller (PM 200). These mixtures were dried and calcined at  $1100^\circ\text{C}$  for 36h in air in a programmable furnace with intermediate grindings. These calcined powders were again milled for 10h. Then the powders were uniaxially pressed into pellets 0.589cm in diameter and 0.262 cm in thickness. The readily formed pellets were sintered for 4h with a heating rate of  $10^\circ\text{C}/\text{min}$  and then cooled to room temperature.

The crystalline phases and lattice parameters of the sintered samples were identified by X-Ray diffractometer (Rigaku) using  $\text{CuK } \alpha$  radiation. Microstructural analysis of the sintered

---

\*Corresponding author: vsharonsamyuktha@gmail.com

samples was performed by SEM and Energy Dispersive X-Ray Spectroscopy (EDS). The dielectric constant, dielectric loss and AC conductivity were measured by LCR meter HIOKI 3252-50 in the frequency range 0.1KHz to 5MHz. The dielectric constant [16] is measured by

$$\varepsilon_r = \frac{C * d}{\varepsilon_0 * A} \quad (1)$$

where C is capacitance of the pellet, d is thickness of the pellet; A is the area of the cross section of the pellet and  $\varepsilon_0$  is the permittivity of free space. The AC conductivity of the samples was estimated from dielectric parameters. The AC conductivity ( $\sigma_{AC}$ ) was calculated using the relation [17,18]:

$$\sigma_{AC} = \omega \varepsilon \varepsilon_0 \tan \delta \quad (2)$$

where  $\varepsilon_0$  is the permittivity of the free space,  $\omega$  is the angular frequency and  $\tan \delta$  is the loss tangent.

### 3. Results and discussions

#### 3.1. XRD analysis

The crystalline structure of  $Mg_{0.1}Ca_{0.9}TiO_3$  ceramic sample was evaluated by XRD analysis at room temperature using Rigaku X-Ray Powder Diffract Meter (Japan) are shown in Fig. 1 and Table 1.

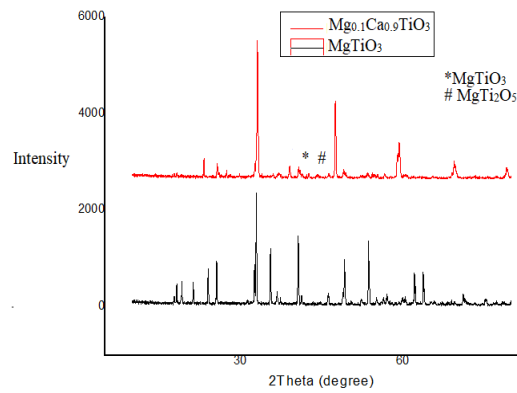


Fig.1 XRD pattern of  $Mg_{0.1}Ca_{0.9}TiO_3$  ceramics

Table 1. XRD profile data of  $Mg_{0.1}Ca_{0.9}TiO_3$  sample.

$2\theta$	d-space $\text{\AA}^0$	FWHM	(h k l)	$D_p$ (nm)
23.26958	3.819539	0.102895	(1 0 0)	82.23
25.71824	3.461158	0.208826	(1 1 1)	40.75
33.09667	2.704464	0.196316	(1 1 2)	44.09
40.70905	2.21459	0.147334	(2 0 2)	60.6
49.01521	1.856968	0.441709	(2 2 1)	20.64
54.70815	1.676423	0.304735	(1 3 1)	30.65
58.9192	1.566249	0.239672	(1 3 2)	39.76
59.29216	1.557284	0.191372	(2 1 1)	49.88
60.57413	1.527358	0.815422	(2 2 3)	11.78

Orthorhombic crystalline structure having single reflection peaks with the exception of few additional phases corresponding to the presence of  $\text{MgTiO}_3$  (MT) and  $\text{MgTi}_2\text{O}_5$  exhibited by the sample is observed. The  $\text{MgTi}_2\text{O}_5$  requires a high sintering temperature of  $1450^\circ\text{C}$ . So second phase  $\text{MgTi}_2\text{O}_5$  was formed as intermediate phase and difficult to eliminate from sample prepared by mixed oxide route [17]. The intensity of the diffraction pattern depends on structure factor shows the XRD data of present sample and the average crystallite size ( $D_p$ ) of  $50.52\text{nm}$  was obtained using Scherer formula [19]

$$D_p = k\lambda/\beta\cos\theta \quad (3)$$

where  $k$  is a constant and is equal to  $0.9$ ,  $\theta$  is diffraction angle,  $\lambda=0.154056\text{ nm}$  ( $\text{CuK}\alpha$ ) and  $\beta$  is full width half maxima. The increase in the ionic radius from  $\text{Mg}^{2+}$  is  $0.65\text{Å}$  [20] to  $\text{Ca}^{2+}$  is  $0.99\text{Å}$  leads to small shift towards lower angles. The dislocation density is calculated by the formula  $\rho=D^{-2}$  where its value is found to be  $3.918\times 10^{14}\text{ m}^{-2}$ . The lattice constants are found to be  $a=5.484465\text{ Å}$ ,  $b=5.443375\text{ Å}$  and  $c=7.529209\text{ Å}$  and Unit cell volume is found to be  $224.777026\text{ (Å)}^3$  are calculated for  $\text{Mg}_{0.1}\text{Ca}_{0.9}\text{TiO}_3$  are in good agreement with the crystallographic parameters.

### 3.2. SEM and EDS results

The surface morphology was studied by Scanning Electron Microscopy. Fig.2 shows SEM images of  $\text{Mg}_{0.1}\text{Ca}_{0.9}\text{TiO}_3$  which have been made at two different spots having  $5000\text{ X}$  and  $10,000\text{X}$  magnifications and in  $5\mu\text{m}$ ,  $10\mu\text{m}$  range respectively. In the images the grains are almost spherical in shape containing homogeneous distribution containing with distinguished boundaries with less porosity have been observed. The average particle size was calculated as  $175\text{nm}$ , using the following ImageJ software. The average grain size was measured to be  $5.31\mu\text{m}$  using the formula given in the equation (4). The increase in grain size is due to sintering which enhances the grain size. This high grain growth when compared with crystalline size computed from XRD may be due to low elastic strain and thus high grain boundary creeping occurs. The concentrations of elements such as Mg, Ca, Ti and O present in ceramic sample were determined by EDS analysis which were shown in the Fig.3 Table 2 illustrates the At%, and Wt% of various elements.

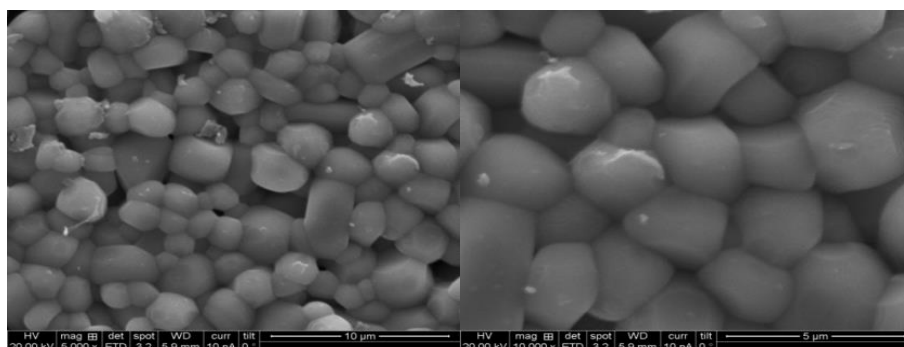


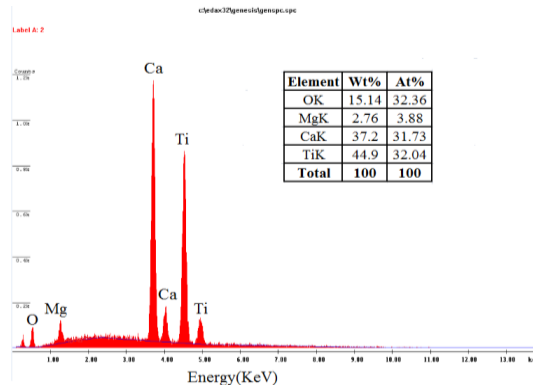
Fig.2. SEM images of  $\text{Mg}_{0.1}\text{Ca}_{0.9}\text{TiO}_3$  sample.

$$\text{Average grain size} = \frac{1.5L}{MN} \quad (4)$$

where  $L$  is  $L$ =the total test line length,  $M$ =the magnification,  $N$ =the total number of intercepts which the grain boundary makes with the line.

Table 2. Shows EDS profile data of  $Mg_{0.1}Ca_{0.9}TiO_3$  sample.

Element	Wt%	At%
OK	15.14	32.36
MgK	2.76	3.88
CaK	37.2	31.73
TiK	44.9	32.04

Fig.3. EDS Spectra recorded from  $Mg_{0.1}Ca_{0.9}TiO_3$  Sample.

### 3.3. Dielectric Studies

The dielectric properties were performed on disks for pure and doped  $MgTiO_3$  in the temperature range from room temperature to  $350^{\circ}C$ . The variation of dielectric constant with temperature at 1kHz frequency is shown in the Fig. 4. The dielectric constant found was 14.5 for  $MgTiO_3$  and for  $Mg_{0.1}Ca_{0.9}TiO_3$  was 90.26 at 1kHz at room temperature. The dielectric constant at different frequencies for the sample  $Mg_{0.1}Ca_{0.9}TiO_3$  were plotted in the figure 5. The dielectric constant is high at low frequency due to the accumulation of charge at the grain boundary and at the interface of electrode sample and electrode which is called space-charge polarization [21, 22]. The dielectric constant decreases as frequency increases due to the gradual deteriorating of the space-charge polarization, indicating the domination of the electronic and atomic contribution. Figure 6 depicts the variation of tangent loss with temperature for  $Mg_{0.1}Ca_{0.9}TiO_3$  ceramic sample at different frequencies ranging from 1kHz, to 1MHz. At low frequency there is increase in dielectric loss with temperature nearly at  $200^{\circ}C$  and then decreases. At higher frequencies the dielectric loss is very low and almost stable. This may be an extrinsic loss dominated by secondary phases, oxygen vacancies, grain sizes and densification. The variation ac conductivity as a function of frequency at different temperatures is plotted in the figure 7. As the temperature goes on increasing, the dielectric relaxation gets thermally activated and hence this can be governed by the Arrhenius equation [23, 24].

$$\sigma = \sigma_0 e^{-\frac{E_a}{K_B T}} \quad (5)$$

where  $K=8.6 \times 10^{-5} eV$ ,  $\sigma_0$ = pre exponential factor, and  $T$ = absolute temperature. In general  $\sigma_{ac}$  can be calculated by the following equation.

$$\sigma_{ac} = \epsilon_o \epsilon_r \omega \tan \delta \quad (6)$$

where  $\epsilon_r$  =dielectric constant,  $\epsilon_0=8.9 \times 10^{-12}$  F/m,  $\omega=2\pi f$  and  $\tan\delta$ = loss tangent. The slopes of the curves attribute activation energies and were attained as 0.643 eV and 0.105 eV at 1 kHz and 1MHz frequencies respectively. This definitely establishes a fact that conductivity increases with increasing frequency and becomes independent of temperature at high frequencies. At lower frequencies the conductivity increases with increase of temperature due to thermal activation process and this may be due to hopping of charge carriers which are bound in the localized states while conductivity decreases with increasing frequencies because of hopping of free charge carriers from one lattice to the other due to electronic and ionic conduction [16]. Another reason could be attributed to the fact that the dopants can introduce defects which may lead to segregate at the grain boundaries due to diffusion process resulting from sintering and cooling processes.

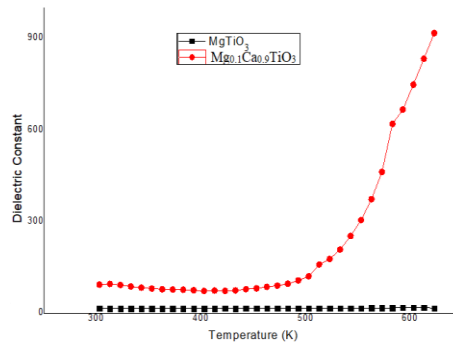


Fig. 4. Variation of Dielectric Constant with Temperature at 1KHz frequency for  $Mg_{(1-x)}Ca_xTiO_3$  samples.

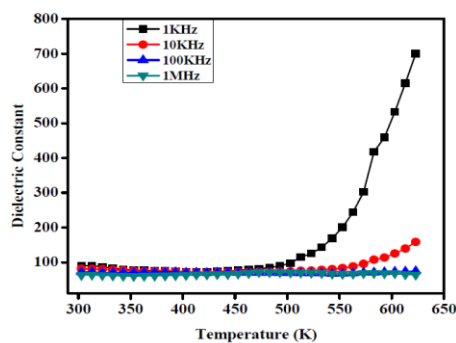


Fig. 5. Variation of Dielectric Constant of  $Mg_{0.1}Ca_{0.9}TiO_3$  with Temperature at Different frequencies.

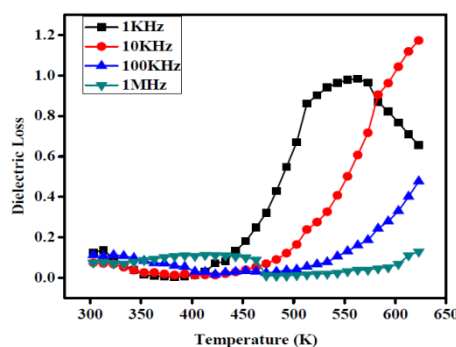


Fig. 6. Variation of Dielectric loss ( $\tan\delta$ ) with Temperature at 1KHz frequency for  $Mg_{0.1}Ca_{0.9}TiO_3$  sample.

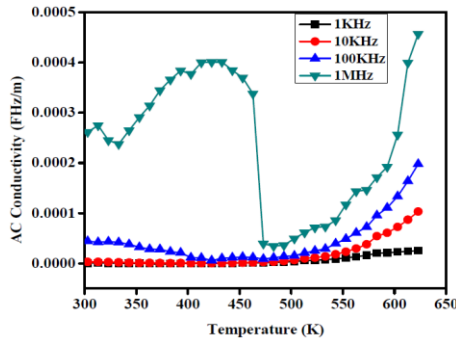


Fig. 7. Variation of ac conductivity of  $Mg_{0.1}Ca_{0.9}TiO_3$  with Temperature at Different frequencies.

**3.4. Electrical Studies**

Figure 8 shows the variation of Thermoemf (E) with temperature. The Seebeck coefficient (thermoelectric power) as a function of temperature of  $Mg_{0.1}Ca_{0.9}TiO_3$  ceramics sintered at  $1200^{\circ}C$  is shown in fig.9. The Seebeck coefficient is positive and increases with increase of temperature revealing that holes are being introduced by Ca addition. At high temperatures the Seebeck coefficient remains constant and later decreased with an overall slope of  $248.78\mu V/K$ . The carrier concentration (n) was calculated for the  $Mg_{0.1}Ca_{0.9}TiO_3$  pellet of thickness 0.262cm and radius 0.589cm as  $0.197 \times 10^{22} \text{ cm}^{-3}$  using the following equation [25].

$$n = \frac{N}{V} \exp\left(\frac{-Se}{K}\right) \tag{7}$$

where  $N=10^{22} \text{ cm}^{-3}$  (Density of states),  
 $V=0.15 \text{ cm}^3$  (Volume of the sample),

$$\frac{k}{e} = 86.4 \mu V/K$$

S=Seebeck Coefficient

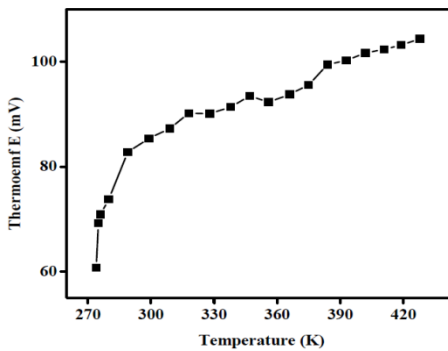


Fig. 8. Variation of Thermoemf with Temperature for  $Mg_{0.1}Ca_{0.9}TiO_3$  sample.

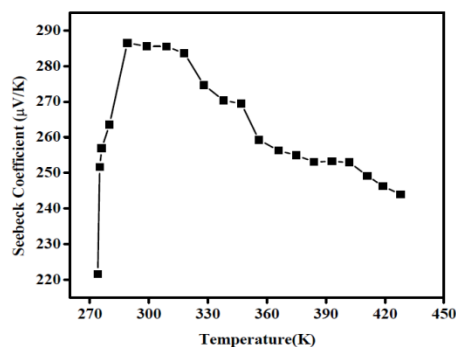


Fig. 9. Variation of Seebeck Coefficient with Temperature for  $Mg_{0.1}Ca_{0.9}TiO_3$  sample.

#### 4. Conclusions

This study reveals that the  $Mg_{0.1}Ca_{0.9}TiO_3$  sample is of Orthorhombic structure except that of few additional phases of  $MgTi_2O_5$  with good homogeneity and crystalline nature by XRD analysis. From the SEM analysis it is revealed that grains are almost spherical in shape and are distributed with less porosity, homogeneously. In the low frequency region the dielectric constant decreases with the frequency where as it shows frequency-independent behaviour in the high frequency region. It is also a high dielectric constant material with low dielectric loss which means it is suitable for microwave applications.

#### References

- [1]. Coondoo, N. Panwar, A. Tomar, A.K. Jha, S.K. Agarwal, Phys. B Condens. Matter. **407** (2012) 4712–4720.
- [2]. N. Rezlescu, E. Rezlescu, Phys. Status Solidi. **23** (1974) 575–582.
- [3]. Z. Wang, J. Tang, Y. Chen, L. Spinu, W. Zhou, L.D. Tung, J. Appl Phys., **95** (11) 7384.
- [4]. H. Wang, Q. Gao, H. Li, M. Gao, B. Han, K. Xia, C. Zhou, ACS Appl. Nano Mater., **1** (2018) 2727–2738.
- [5]. S.K. Pendyala, K. Thyagarajan, A. GuruSampath Kumar, L. Obulapathi, J. Aust. Ceram. Soc. **54** (2018) 467–473.
- [6]. V. Sharon Samyuktha, A. Guru Sampath Kumar, T. Subba Rao, R. Padma Suvarna, Mater. Today Proc., **3** (2016): pp. 1768–1771.
- [7]. M. Javed, S. Hussain, Dig. J. Nanomater. Biostructures. **15** (2020) 217–230.
- [8]. S. Roy, S. Bandyopadhyay, D. Chakravorty, J. Mater. Sci. Lett. **15** (1996) 1872–1874.
- [9]. M. Marie, S. Mandal, O. Manasreh, Sensors, **15** (2015) 18714–18723.
- [10]. S. Karadaş, S.A. Yerişkin, M. Balbaş, Y. Azizian-Kalandaragh, J. Phys. Chem. Solids. **148** (2021) 4587.
- [11]. C.L. Huang, Y.W. Tseng, IEEE Trans. Dielectr. Electr. Insul. **21** (2014) 2293–2300.
- [12]. K.P. Surendran, A. Wu, P.M. Vilarinho, V.M. Ferreira, K.P. Surendran, A. Wu, P.M. Vilarinho, V.M. Ferreira, J. Appl. Phys., **107** (2010) 0–8.
- [13]. S.K.S. Basha, G.S. Sundari, K.V. Kumar, M.C. Rao, J. Inorg. Organomet. Polym. Mater. **27** (2017) 455–466.
- [14]. A. Sinica, comparison of various preparation methods, **139** (1996) 75–85.
- [15]. H.J. Jeon, S.G. Lee, H. Kim, J.S. Park, Appl. Surf. Sci. **301** (2014) 358–362.
- [16]. P. Sivakumar, K. Thyagarajan, A.G. Kumar, Dig. J. Nanomater. Biostructures. **13** (2018) 1117–1122.
- [17]. M. Maddaiah, A.G. Kumar, L. Obulapathi, T.S. Sarmash, K.C. Babu Naidu, D.J. Rani, T.S. Rao, Dig. J. Nanomater. Biostructures. **10** (2015) 155–159.
- [18]. O.B. Qader, Y. Ruisheng, K. Chaudhary, F.F. Muhammad, M.Y. Yahya, M.R. Ahmad, F.D. Ismail, J. Ali, Dig. J. Nanomater. Biostructures. **15** (2020) 25–32.

- [19]. A. GuruSampath Kumar, L. Xuejin, Y. Du, Y. Geng, X. HongJ. Alloys Compd. **798** (2019) 467–477.
- [20]. P. Gogoi, P. Srinivas, P. Sharma, D. Pamu, J. Electron. Mater. **45** (2016) 899–909.
- [21]. K.C.B. Naidu, W. Madhuri, J. Magn. Magn. Mater. **420** (2016) 109–116.
- [22]. R. Mohammadi, R.S. Azis, A. Zakaria, N.H. Isa, N.K. Saat, N. Mokhtar, F.D. Muhammad, Dig. J. Nanomater. Biostructures. **14** (2019) 1105–1113.
- [23]. K. Miura, K. Fujiwara, J. Shiogai, T. Nojima, A. Tsukazaki, J. Appl. Phys., **127** (2020) 103903.
- [24]. D.J. Rani, A.G.S. Kumar, L. Obulapathi, T.S. Rao, Trans. Dielectr. Electr. Insul. **26** (2019) 1134–1138.
- [25]. V.S. Samyuktha, A. Guru, S. Kumar, T.S. Rao, R.P. Suvarna, Mater. Today Proc. **3** (2016) 1768–1771.